

Gaussian Process Regression for Binned Data

Michael Thomas Smith · Mauricio A Álvarez · Neil D Lawrence*

Received: date / Accepted: date

Abstract Many datasets are in the form of tables of binned data. Performing regression on these data usually involves either reading off bin heights, ignoring data from neighbouring bins or interpolating between bins thus over or underestimating the true bin integrals.

In this paper we propose an elegant method for performing Gaussian Process (GP) regression given such binned data, allowing one to make probabilistic predictions of the latent function which produced the binned data.

We look at several applications. First, for differentially private regression; second, to make predictions over other integrals; and third when the input regions are irregularly shaped collections of polytopes.

In summary, our method provides an effective way of analysing binned data such that one can use more information from the histogram representation, and thus reconstruct a more useful and precise density for making predictions.

Keywords Regression · Gaussian Process · Integration

This work has been supported by the Engineering and Physical Research Council (EPSRC) Research Project EP/N014162/1. We also thank Wil Ward for his assistance and suggestions.

*Work conducted while at the University of Sheffield.

Michael Thomas Smith
Department of Computer Science
University of Sheffield
E-mail: m.t.smith@sheffield.ac.uk

Mauricio A Álvarez López
Department of Computer Science
University of Sheffield
E-mail: mauricio.alvarez@dcs.shef.ac.uk

Neil D Lawrence
Department of Computer Science
University of Sheffield
E-mail: neil@sheffield.ac.uk

1 Introduction

Consider the following problem. You want to use a dataset of children's ages and heights to produce a prediction of how tall a child of 38 months will be. The dataset has been aggregated into means over age ranges: e.g. those aged 24 to 36 months have an average height of 90cm, those aged 36 to 48 months, 98cm, etc.

A naive approach would be to simply read off the age range's mean. A slightly more advanced method could interpolate between bin centres. The former method fails to use the data in the neighbouring bins to assist with the prediction, while the latter will produce predictions inconsistent with the dataset's totals. Ideally we would have access to the original dataset, however binning such as this is ubiquitous, sometimes for optimisation (for storage or processing, for example hectad counts in ecology, annual financial reports, traffic counts), sometimes as an attempt to preserve privacy (for example geographical and demographic grouping in the census) and sometimes due to the data collection method itself (camera pixels or fMRI voxels; survey selection, as in section 4.4; or rain-gauge measurements taken each hour). The examples in this paper cover some of these use cases, although many others exist. We also demonstrate how this method can be combined with differential privacy (DP), to provide a simple method for performing DP-regression.

In this paper, we propose a method for performing Gaussian Process (GP) regression given such binned data. Gaussian Processes are a principled probabilistic method for performing regression given uncertain training data inputs. Put simply they provide a way of describing how one believes data across input space is correlated, and thus make predictions using previously given training data. We show how one can find the cor-

relation between a cuboid region’s integral and a single point. In essence, the histogram we are working with can be considered as a simple form of density estimation. We attempt to extract as much information as possible from the histogram representation, and reconstruct a more useful and precise density. We will later refer to the analytically derived kernel as the *integral kernel*.

The analytical method described only applies when the boundaries of the integral are independent of one another (i.e. the volume to be integrated over is a cuboid) which often occurs in real datasets, for example in population surveys one might bin people into age ranges and income ranges. However there are many cases where the bins are non-cuboid. An obvious example is that of census tracts, which often follow complicated paths. Kyriakidis (2004) handle this by approximating the volumes with sets of points, over which the covariance is computed. We briefly re-examine this method (including the problem of point placement and hyperparameter optimisation), extending it to instead use a set of hyperrectangles to approximate the volumes instead.

The analytical derivation is based on work by Alvarez et al (2009) in which dynamical systems are modelled using a Gaussian process. A related article is that of Ažman and Kocijan (2005) in which derivatives of a function are observed (rather than the function itself). This was later used to enforce monotonicity in Riihimäki and Vehtari (2010). In the current paper we operate in the opposite direction, and assume we have observations of a collection of definite integrals of a latent function.

Unlike probabilistic integration (O’Hagan, 1991), we are not trying to integrate a function, but rather have been given the integrals of an unknown ‘latent’ function and wish to reconstruct this unknown function.

There is a slight relationship with the combining of basis functions in functional analysis. In Ramsay (2006, equation 16.3), the authors describe how a new kernel is created by summing over the basis functions of two one-dimensional bases, a little as we integrate over the (effectively infinite, for a GP) basis functions that lie over the domain being integrated.

We first derive both the analytical and approximate forms of the kernel, then demonstrate the methods on a series of simulated and real datasets and problems.

2 Analytical Derivation

To begin we consider the analytical formulation in which we believe that there is a latent function that has been integrated to provide the outputs in the training data. We assume, for now, that we want to make predictions for this latent function. To proceed via Gaussian process

regression (Williams and Rasmussen, 2006) we assume that there is some *latent function*, $f(t)$, that represents the values of weights as a function of age. The summary measures (average over age ranges) can then be derived by integrating across the latent function to give us the necessary average. Importantly, if the latent function is drawn from a Gaussian process then its integral is also *jointly* drawn from the same Gaussian process. This allows us to analytically map between the aggregated measure and the observation of interest.

To summarise, we assume that a second function, $F(s, t)$, describes the integral between the ages s and t of $f(\cdot)$ and we are given observations, $y(s, t)$, which are noisy samples from $F(s, t)$.

A Gaussian process assumption for a function specifies that for a set of points, the outputs should be jointly distributed as a Gaussian density with a particular mean and covariance matrix. A Gaussian density has the property that any linear combination of its samples will, in turn, be jointly distributed as Gaussian with the original density. Similarly for a Gaussian process, any *linear operator* (such as integration) applied to the original function will lead to a joint Gaussian process over the result of that linear operator and the original function. In other words there will be a joint Gaussian process between the two functions $f(t')$ and $F(s, t)$. Such a Gaussian process is specified, *a priori*, by its mean function and its covariance function. The mean function is often taken to be zero (although non-zero mean functions are easily incorporated into the framework) but it is the covariance function where the main interest lies.

To construct the joint Gaussian process posterior we need expressions for the covariance between values of $f(t)$ and $f(t')$, values of $F(s, t)$ and $F(s', t')$ (i.e. the covariance between two integrals) and the ‘cross covariance’ between the latent function $f(t')$ and the output of the integral $F(s, t)$. Where t, t', s and s' specify input locations.

For the underlying latent function we assume that the covariance between the values of the latent function $f(\cdot)$ is described by the exponentiated quadratic (EQ) form,

$$k_{ff}(u, u') = \alpha e^{-\frac{(u-u')^2}{l^2}},$$

where α is the scale of the output and l is the (currently) one-dimensional length-scale.¹ We are given training points from the integral $F(s, t) = \int_s^t f(u) du$. Reiterating the above, if $f(u)$ is a GP then $F(s, t)$ is also a GP with a covariance we can compute by integrating the covariance

¹ Note that there is a $\sqrt{2}$ difference between our length-scale and that normally defined, this is for convenience in later integrals.

of $f(u)$,

$$k_{FF}((s, t), (s', t')) = \alpha \int_s^t \int_{s'}^{t'} k_{ff}(u, u') du' du.$$

Substituting in our EQ kernel, and integrating,

$$\begin{aligned} k_{FF}((s, t), (s', t')) &= \frac{1}{2} \sqrt{\pi} l \alpha \left[(s' - s) \operatorname{erf}\left(\frac{s - s'}{l}\right) \right. \\ &+ (s - t') \operatorname{erf}\left(\frac{s - t'}{l}\right) + s' \operatorname{erf}\left(\frac{s' - t}{l}\right) \\ &+ t \operatorname{erf}\left(\frac{t - s'}{l}\right) + (t - t') \operatorname{erf}\left(\frac{t' - t}{l}\right) \\ &\left. + \frac{l}{\sqrt{\pi}} \left(-e^{-\frac{(s-s')^2}{l^2}} + e^{-\frac{(s-t')^2}{l^2}} + e^{-\frac{(s'-t)^2}{l^2}} - e^{-\frac{(t-t')^2}{l^2}} \right) \right], \end{aligned} \quad (1)$$

where $\operatorname{erf}(\cdot)$ is the Gauss error function. For ease of interpretation and later manipulation we rewrite this as,

$$\begin{aligned} k_{FF}((s, t), (s', t')) &= \alpha \frac{l^2}{2} \\ &\times \left[g\left(\frac{t - s'}{l}\right) + g\left(\frac{t' - s}{l}\right) \right. \\ &\quad \left. - g\left(\frac{t - t'}{l}\right) - g\left(\frac{s - s'}{l}\right) \right] \end{aligned} \quad (2)$$

where we defined $g(z) = z\sqrt{\pi}\operatorname{erf}(z) + e^{-z^2}$.

Because we are interested in computing a prediction for the latent function (i.e. the density) that's been integrated, it would be useful to have the cross-covariance between F and f . If we assume that the joint distribution of F and f is normal, we can calculate the cross-covariance,

$$k_{Ff}((s, t), (t')) = \frac{\sqrt{\pi}l}{2} \left(\operatorname{erf}\left(\frac{t - t'}{l}\right) + \operatorname{erf}\left(\frac{t' - s}{l}\right) \right). \quad (3)$$

When using this 'integral kernel' in a real GP regression problem we are likely to need to select appropriate hyperparameters. Typically this is done using gradient descent on the negative log marginal-likelihood, L , with respect to the hyperparameters. In this case, we need the gradient of K_{FF} wrt l and α (respectively, the length-scale and variance of the latent EQ function).² Defining

² These gradients are then multiplied by $\frac{\partial L}{\partial K_{FF}}$ by the GP framework to give the gradients $\frac{\partial L}{\partial l}$ and $\frac{\partial L}{\partial \alpha}$.

$h(z) = \frac{z\sqrt{\pi}}{2} \operatorname{erf}(z) + e^{-z^2}$, we can write the gradient as

$$\begin{aligned} \frac{\partial k_{FF}((s, t), (s', t'))}{\partial l} &= \alpha l \\ &\times \left[h\left(\frac{t - s'}{l}\right) + h\left(\frac{t' - s}{l}\right) \right. \\ &\quad \left. - h\left(\frac{t - t'}{l}\right) - h\left(\frac{s - s'}{l}\right) \right]. \end{aligned} \quad (4)$$

and $\frac{\partial k_{FF}}{\partial \alpha}$ is simply the expression for k_{FF} in (2) with the initial α removed.

The same idea can be used to extend the input to multiple dimensions. If we specify that each dimension's kernel function contains a unique lengthscale parameter, with a bracketed kernel subscript index indicating these differences, we can express the new kernel as the product of our one dimensional kernels,

$$k_{FF}((\mathbf{s}, \mathbf{t}), (\mathbf{s}', \mathbf{t}')) = \prod_i k_{FF(i)}((s_i, t_i), (s'_i, t'_i)),$$

with the cross covariance given by

$$k_{Ff}((\mathbf{s}, \mathbf{t}), (\mathbf{s}', \mathbf{t}')) = \prod_i k_{Ff(i)}((s_i, t_i), (s'_i, t'_i)).$$

3 Arbitrary Polygon Shapes

The above product of kernels assumes that we integrate over the whole domain between t_i and t'_i for each dimension i , giving a Cartesian product of intervals. This constrains us to regions consisting of rectangles, rectangular cuboids or hyperrectangles. Thus if our input regions are described by polytopes³ that are not hyperrectangles aligned with the axes, then the above computation is less immediately tractable, as the boundaries of the integral kernels will interact. For specific cases one could envisage a change of variables, but for an arbitrary polytope we need a numerical approximation. Kyriakidis (2004) propose a numerical approximation that mirrors the exact analytical methods in this paper. Specifically they find an approximation to the double integral (2) of an underlying kernel (equation 5 in the reference). Given a uniformly random set of locations (x_i and x'_i) in each polygon, one sums up the covariances, $k_{ff}(x_i, x'_i)$, for all these pairings. Then to correct for the volumes of the two regions one divides by the number of pairings (NN') and multiplies by the product of their areas/volumes (A and A') to get an approximation to the integral,

³ A polytope is the generalisation of a polygon to arbitrary numbers of dimensions.

$$k_{FF}(X, X') \approx \frac{AA'}{NN'} \sum_{i=1}^N \sum_{j=1}^{N'} k_{ff}(x_i, x'_j).$$

Algorithm 1 Pick a random point inside a polytope.

Require: \mathcal{T} , the polytope we want to fill with samples - described by a list of $d \times n$ matrices defining simplexes. d spatial dimensions and $n = d + 1$ vertices.

Require: ρ , density of points (points per unit volume)

```

1: function GETUNIFORMSAMPLES( $\mathcal{T}$ ,  $\rho$ )
2:   for SIMPLEX,  $\mathcal{S}$  in  $\mathcal{T}$  do
3:      $V \leftarrow \text{CALCVOLUME}(\mathcal{S})$ 
4:     for  $0 \leq i < V\rho$  do
5:        $P \leftarrow P \cup \text{SIMPLEXRANDOMPOINT}(\mathcal{S})$ 
6:     end for
7:   end for
8: end function
9:
10: function CALCVOLUME( $\mathcal{S}$  made of vertices  $v_0 \dots v_{n-1}$ )
     $\triangleright$  modified from Stein (1966)
    return  $|\frac{1}{d!} \det [v_1 - v_0, v_2 - v_0, \dots, v_{n-1} - v_0]|$ 
11: end function
12:
13: function SIMPLEXRANDOMPOINT( $\mathcal{S}$ )
     $\triangleright$  Algorithm duplicated from Grimme (2015)
14:    $z \leftarrow [1] \# \text{uniform}(d) \# [0]$   $\triangleright$  see footnote†
15:    $l_i \leftarrow z_i^{1/(n-i)} \quad 1 \leq i \leq n$ 
    return  $\sum_{i=1}^n (1 - l_i) (\prod_{j=1}^i l_j) v_i$ 
16: end function

```

[†]uniform(d) selects d uniformly random numbers. # is the concatenation operator.

Note that an advantage of this numerical approximation is the ease with which alternative kernels can be used. Their paper does not address the issue of point placement or hyperparameter optimisation. We decided the most flexible approach was to consider every object as a polytope. Each object is described by a series of S simplexes, and each simplex is described by $d + 1$ points (each consisting of d coordinates). Selecting the simplexes is left to the user, but one could build a 3d cube (for example) by splitting each side into two triangles and connecting their three points to the cube’s centre, thus forming 12 simplexes, requiring $12 \times 4 \times 3 = 144$ input values. Next, for every input polytope we place points. We summarise a method for point placement in algorithm 1 which describes how one might select points distributed uniformly within each polytope. Finally, for each pair of points between each pair of polytopes we compute the covariance and the gradient of the kernel with respect to the hyperparameters. To compute the gradient of the likelihood with respect to the hyperparameters, we need to compute the gradients for all the $N \times N'$ point pairings, using the kernel, $k_{ff}(\cdot, \cdot)$, of the

latent function, and average (taking into account the areas (A and A') of the two polygons);

$$\frac{\partial L}{\partial \theta} = \frac{AA'}{NN'} \sum_{i=1}^N \sum_{j=1}^{N'} \frac{\partial k_{ff}(x_i, x_j)}{\partial \theta} \frac{\partial L}{\partial K}.$$

3.1 Hyperrectangle Numerical Approximation

One obvious proposal is to combine the numerical and analytical methods. We also generalise the above method to handle the covariance between a pair of sets of polytopes. Specifically, rather than approximate a set of polytopes with points, one could, conceivably achieve a higher accuracy by replacing the points with the same number of hyperrectangles, placed to efficiently fill the polytopes. As with the point method, but with hyperrectangles; we compute the covariance k_{FF} between all pairings of hyperrectangles from the different sets of polytopes and then sum these to produce an estimate for the covariance between the two sets of polytopes (potentially correcting for the volume of the two sets of polytopes if the two sets of hyperrectangles do not completely fill them). Specifically, we compute,

$$k_{FF}(X, X') \approx \sum_{i=1}^N \sum_{j=1}^{N'} \frac{A_i A'_j}{a_i a'_j} k_{FF}(x_i, x'_j).$$

where A_i refers to the volume of the polytope associated with hyperrectangle i (note other hyperrectangles may also be associated with that polytope), and a_i is the sum of the volumes of all the hyperrectangles being used to approximate the same polytope. Thus their ratio gives us a correction for the hyperrectangle’s volume shortfall.

The placement of the hyperrectangles is a more complex issue than the placement of the points in the previous section. For the purposes of this paper we use a simple greedy algorithm for demonstration purposes. Other work exists on the time complexity and efficient placement of rectangles to fill a polygon, although many either allow the rectangles to be non-axis-aligned or requires the polygon to be an L shape (Iacob et al, 2003) or orthogonal, or are only for a single rectangle (Daniels et al, 1997) in a convex polygon Knauer et al (e.g. 2012); Alt et al (e.g. 1995); Cabello et al (e.g. 2016). We found the straightforward greedy algorithm to be sufficient.

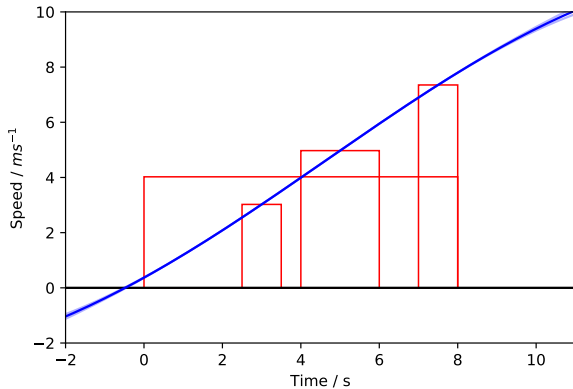


Fig. 1 Illustration of how the robot’s speed can be inferred from a series of observations of its change in location, here represented by the areas of the four rectangles. The blue lines indicate the posterior mean prediction and its 95% confidence intervals.

Start location / m	End location / m	Time
0	8	32.18
2.5	3.5	3.02
4	6	9.94
7	8	7.35

Table 1 Simulated observations of robot travel distances. Figure 1 illustrates these observations with rectangle areas.

4 Results

4.1 Speed Integration Example

Before looking at a real data example, we illustrate the kernel with a simple toy example. We want to infer the speed of a robot that is travelling along a straight line. The distance it has travelled between various time points has been observed, as in table 1. A question we might ask, how fast was the robot moving at 5 seconds? We enter as inputs the four integrals. We select the lengthscale, kernel variance and Gaussian noise scale by maximising the log marginal likelihood, using gradient descent. We now can make a prediction of the latent function at five seconds using standard GP regression. Specifically the posterior mean and variances are estimated to be,

$$\bar{f}_* = \mathbf{k}_{F_*}^\top (K_{FF} + \sigma^2 I)^{-1} \mathbf{y} \quad (5)$$

$$V[f_*] = k_{**} - \mathbf{k}_{F_*}^\top (K_{FF} + \sigma^2 I)^{-1} \mathbf{k}_{F_*} \quad (6)$$

Where K_{FF} is the covariance between pairs of integrals, \mathbf{k}_{F_*} is the covariance between a test point in latent space and an integral. σ^2 is the model’s Gaussian noise variance. \mathbf{y} are the observed integral outputs and k_{**} is the variance for the latent function at the test point.

The optimal hyperparameters that maximise the log marginal likelihood, are for the kernel to have variance of $54\text{m}^2\text{s}^{-2}$ and lengthscale 19s, with a very small model Gaussian noise. The relatively long lengthscale means the speed increases roughly linearly. One can see that this is appropriate for the observations made, in which the rate that distance is covered increases linearly with time.

Figure 1 illustrates the four observations as the areas under the four rectangles, and shows the posterior prediction of the GP. To answer the specific question above, the speed at $t = 5\text{s}$ is estimated to be $4.97 \pm 0.00024\text{ms}^{-1}$ (95% CI).

We now look at several examples of real data. In Section 4.2 we consider a histogram of people’s ages. We have, however, added noise to the data to ensure the privacy of the individuals using the framework of differential privacy to illustrate the relative noise immunity that the integral kernel appears to achieve. In Section 4.3 we consider another histogram example, but this time with a higher dimensional input. In Section 4.4 we extend the method to predict other integrals (not just densities). Finally in Sections 4.5 and 4.6 we consider non-rectangular input volumes and compare numerical approximations for GP regression.

4.2 Differentially Private Age Data

We consider the age distribution of 255 people from a single output area (E00172420) from the 2011 UK census.⁴ We also make this histogram differentially private, to demonstrate the improved noise immunity of the new method. We group the people into a histogram with equal ten year wide bins, and add differentially private noise using the Laplace mechanism (Dwork and Roth, 2014, section 3.3). Specifically we take samples from a scaled Laplace distribution and add these samples to the histogram’s values. The Laplace noise is scaled such that the presence or absence of an individual is provably difficult to detect, using ϵ -DP Laplace mechanism. One can increase the scale of the noise (by reducing ϵ) to make it more private. Or decrease ϵ , sacrificing privacy for greater accuracy. The aim is to predict the number of people of a particular age. We use three methods; simply reading off the bin-heights, fitting a standard GP (with an EQ kernel) to the bin centroids, or using a GP with the integral kernel.

Figure 2 demonstrates these results. Note that the GP with an integral kernel will attempt to model the

⁴ a peak of students at age 18 was removed, so the graph only includes the permanent residents of the area.

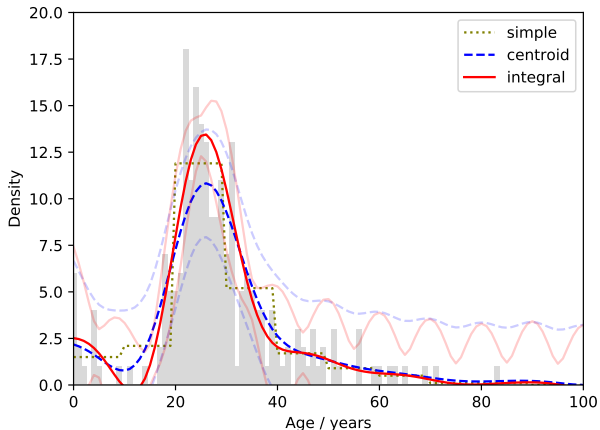


Fig. 2 Various fits to an age histogram of 255 people in which the data has been aggregated into ten-year wide bins (with $\epsilon=1$ Laplace differential privacy noise added), with the original (non-DP data) plotted as grey bars. The dotted, orange line uses the bin heights to make predictions directly. The dashed, blue line fits an EQ GP to the centroids of the bins. The red solid line is the prediction using the integral kernel. The 95% confidence intervals are indicated with fainter lines.

area of the histogram, leading to a more accurate prediction around the peak in the dataset.

To explore the interaction of the methods with the addition of noise to the data, we manipulate the scale of the DP noise (effectively increasing or decreasing the scale of the Laplace distribution) and investigate the effect on the RMSE of the three methods. Remember that decreasing the value of ϵ makes the prediction more private (but more noisy). This is not cross-validated leave-one-out, as the use-case includes the test point in the aggregation.

Table 2 illustrates the effect of the DP noise scale on the RMSE. We find that the integral method performs better than the others for all noise-scales tested. Intriguingly the simple method seems to be less affected by the addition of DP noise, possibly as the two GP methods effectively try to use some aspect of the gradient of the function, an operation which is vulnerable to the addition of noise. The integral method seems particularly useful in the most commonly used region of $0.2 \leq \epsilon \leq 2$, with meaningful reductions in the RMSE of up to 13%.

4.3 Citibike Data (4d hyperrectangles)

The above example was for a one-dimensional dataset. We now consider a 4d histogram. The New York based citibike hire scheme provides data on the activities of its users. Here we use the start and end locations (lat and long) to provide the four input dimensions, and try to

ϵ	Simple	Centroid	Integral	95% CI
0.05	5.86	3.11	3.04	0.06
0.1	5.36	2.45	2.19	0.03
0.2	5.21	2.07	1.78	0.03
0.5	5.17	1.90	1.65	0.02
1.0	5.16	1.83	1.63	0.01
2.0	5.16	1.78	1.63	0.01
5.0	5.16	1.77	1.63	< 0.01
∞	5.16	1.76	1.63	

Table 2 RMSE for all 100 age bins, for the simple (directly read off histogram), centroid (RBF GP fit to bin centres) and integral methods, for various levels of differential privacy. Computed RMSE using 500 DP samples. 10,000 bootstrap resamples used to compute 95% CI estimate, value quoted is largest of three columns for simplicity.

predict journey duration as the output. To demonstrate the integral kernel we bin these data into a 4-dimensional grid, and find the mean of the data points that lie within each bin. To investigate the integral kernel’s benefits we vary the number of bins and the number of samples in these bins. As before we compare against an alternative method in which we fit a GP (using an EQ kernel) to the centroids of the bins. Note that bins that contain no datapoints were not included as training data (as their mean was undetermined). To ensure no privacy loss occurs from this particular training set, in this section we chose the two models’ hyperparameters using a grid search on another sample of citibike data. As in the previous section we are interested in being able to predict the individual values used to make the model.

Table 3 illustrates these results. One can see obvious features; more samples leads to more accurate predictions and very large or very small numbers of bins causes degradation in the prediction accuracy. However, most interesting is how these interact with the two methods. First we can see that in all cases, the integral method does better than the centroid method, however its improvement is most pronounced in those cases where the data is sparse (such as when there are few training points and/or large numbers of bins for them to be distributed into). In these cases the bin means are effectively quite noisy, leading to a similar improvement as in the previous section, when using the integral kernel. Specifically, these first two experiments suggest that when there are many data points the two methods are fairly comparable, but the integral kernel is of greatest utility when there either are few samples (as shown in table 3), or they contain considerable noise (as shown in table 2, for low values of ϵ).

Samples	Number of bins							
	1 ⁴		3 ⁴		7 ⁴		15 ⁴	
	centroid	integral	centroid	integral	centroid	integral	centroid	integral
160	495.6	491.3	438.1	435.5	524.6	452.6	739.4	489.1
320	493.5	490.9	441.7	433.6	414.7	381.8	590.2	481.5
640	497.0	496.7	443.9	410.4	401.6	383.8	565.0	479.4
1280	497.6	497.2	438.0	396.0	381.1	373.5	513.5	473.5
2560	497.8	497.4	444.8	399.3	369.4	361.0	460.7	456.7

Table 3 Mean Absolute Error in predictions of journey duration (in seconds) for the citibike dataset using the integral and centroid methods, over a variety of sample counts and bin counts. 1000 randomly chosen journeys were used in the test set, experiment performed once for each configuration.

	Method			
	Integral		Centroid	
RMSE	126.3	± 10.74	223.1	± 14.88
MAE	73.1	± 4.52	143.5	± 7.51

Table 4 RMSE and MAE for 1998 randomly generated audience survey requests. 95% CIs for these statistics was calculated using non-parametric Monte Carlo bootstrapping with 100,000 samples with replacement.

Number of Points	RMSE	MAE
5	14797	5383
10	13539	4687
20	12657	4120
40	12816	3914
80	13751	3990
160	14706	4129

Table 5 Number of integration approximation points for shape integral method, and the effect this has on the RMSE and MAE of the output area density predictions (population density, people per km²). Reported RMSE and MAE based on average of twenty point placement iterations, 95% CI are less than ±0.6%. Lengthscale = 50m.

4.4 Audience Size Estimation (predicting integrals not densities)

We may also wish to produce predictions for new bins. A motivating, real, example is as follows. Imagine you work for a market research company and have a cohort of citizens responding to your surveys. Each survey requires a particular audience answers it. For example the company’s first survey, in January, required that respondents were aged between 30 and 40 of any income. They had 320 replies. In February a second survey required that the respondents were aged between 25 and 35 and earned at least \$30k, and had 210 replies. In March their third survey targeted those aged 20 to 30 with an income less than \$40k. How many respondents might they expect? The latent function is population density across the age and income axes, while the outputs are population counts. We can use the same expressions, (2 & 3), as described at the start of Section 2 but use K_{FF} instead of K_{Ff} when making predictions (the inputs at the test points now consist of the boundaries of an integral, and not just the location to predict a single density). Figure 3 illustrates this with a fictitious set of surveys targeting sub-groups of the population.

We simulated a population of 5802 survey-takers by sampling from the US census bureau’s 2016 family income database. We distribute the start dates randomly, with a skew towards younger participants. For the example in figure 3 we computed a prediction for the test region using the integral kernel. We compared this to a model in which the counts had been divided by the volumes of the cuboids to estimate the density in each, and

used these with the centroid locations to fit a normal GP (with an RBF kernel) to estimate the density (and hence count) in the test cuboid. For this case we found that both methods underestimated the actual count (of 1641). The centroid method predicted 1263 (95% CI: 991-1535), while the new integral method predicted 1363 (95% CI: 1178-1548). The shortfalls are probably due to the skew in the participant start times towards the older portion. The previous training cuboids would have had lower densities, leading to the underestimates here. Intriguingly the new method still produces a more accurate prediction.

To test this more thoroughly, we simulate 1998 sets of surveys (between 6 and 19 surveys in each set) over this data, and compare the RMSE (and MAE) of the two methods when predicting the number of respondents to a new survey. Table 4 shows that the integral method produces more accurate results in this simulated dataset.

4.5 Population Density estimates (2d non-rectangular disjoint inputs)

In earlier sections we assumed rectangular or cuboid input regions in the training set. However many datasets contain more complicated shapes. In this section we briefly apply the numerical approximation devised by Kyriakidis (2004) and extended in section 3. In this

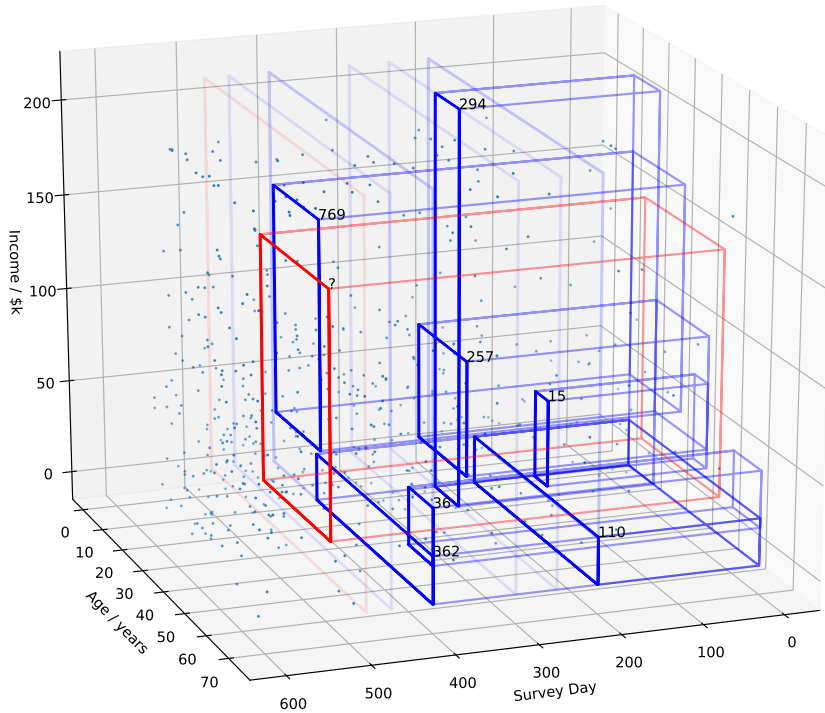


Fig. 3 A demonstration of the audience-size estimation problem. Within the 3d volume lie the individuals that make up the population subscribed by the company, the date they joined is represented by a dot. Seven previous surveys (in blue) have been performed over a growing group of clients. Each survey occupies a cuboid representing the possible individuals that will take part. It extends across the age and income that is included in the survey and backwards from the date the survey was conducted, to include all those participants that have signed up by the survey date. Each volume is labelled with the number of people which took part in each survey. In red is a new survey we want to estimate the count for.

example we use the population density of areas from the UK census. In particular those output areas containing areas lying within a 16km^2 square, centred at Easting/Northing 435/386 km (Sheffield, UK). We assume, for this demonstration, that we are given the total population of a series of 40 subsets of these output areas (the output areas have been allocated to these sets uniformly and randomly). This simulates a common situation in which we know the aggregate of various subpopulations. The task then is to predict the population density of the individual output areas that make up the aggregates. We use 40 approximation points for each set of training polygons. Figure 4 demonstrates example placement results, while Table 5 demonstrates the effect of changing the number of points on the RMSE and MAE. Intriguingly the error increased above a certain point density. The limited number of points maybe acting as a regulariser. As a comparison we found the centroids of the training regions, and used these as inputs to a standard GP (with EQ kernel). We found repeated resampling of the approximation points in the approximation caused problems with the gradient descent algorithm. Instead

	Method	
	Integral	Centroid
RMSE	12773 ± 54	17038.2
MAE	3906 ± 8	5282.5

Table 6 RMSE and MAE for the census example. Values are people per km^2 . Errors are 95% CI based on twenty samples. Forty training points used. Lengthscale = 50m.

we performed a grid search over the hyperparameters on a region centred at Easting/Northing 331.5/188.5 km (Cardiff, UK).⁵ The figure in the supplementary material illustrates the predictions made by the two methods. Neither do particularly well, underestimating most regions. However we found that the point approximation method was able to produce more accurate predictions of the two (see table 6).

⁵ After the grid search the lengthscales for the integral and centroid models were 0.05km and 0.5km respectively.

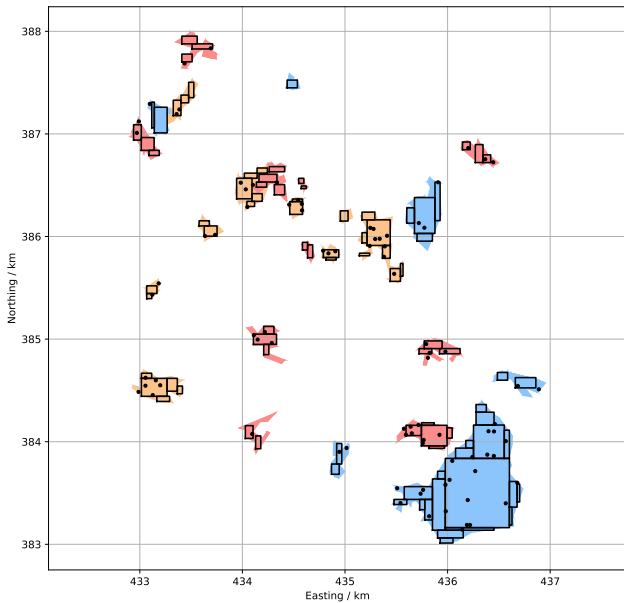


Fig. 4 Example of both rectangular and point approximation to three sets of polygons (from the census output areas of Sheffield). With approximately 30 rectangles or points used for each set.

4.6 Rectangular numerical approximation (2d non-rectangular disjoint inputs)

As described in Section 3.1 we can combine the numerical and analytical solutions by filling the polygons with rectangles, rather than with just points, and use our integral kernel to compute the covariances between the pairs of rectangles and sum the covariances just as with the point method.

Table 7 shows the MAE when computing the covariance between the three sets of polygons in figure 4. Using the rectangle approximation reduces the error by approximately 4 times, for the same number of training points.

Number of points or rectangles	Mean Abs Error	
	Points	Rectangles
16	0.0197	0.0049
32	0.0084	0.0018
64	0.0007	0.0002
128	0.0004	< 0.00015

Table 7 Mean Absolute Error in estimates of the covariance matrix values between the three sets of polygons illustrated in figure 4. The estimated 95% error is ± 0.0001 due to uncertainty in true covariance. Isotropic RBF kernel, lengthscale = 1km.

We experimented briefly at higher dimensions, looking at the estimates of the covariance between a pair of 4-dimensional hyperspheres of radii one and two placed with centres 3 apart, so just touching. Using an isotropic RBF kernel (lengthscale=2.0) we compared ten points to ten rectangles in each sphere and found that the estimated covariance using points (instead of hyperrectangles) had roughly double the MAE (specifically the correct value was 314, with MAEs for points and rectangles were 50.0 and 25.1 respectively).

5 Discussion

In this paper we have derived both an analytical method for inference over cuboid integrals and an approximate method for inference over arbitrary inputs consisting of arbitrary sets of polytopes. In all the experiments, the integral kernels were able to improve on widely used alternatives. However, the improvement was most pronounced when the training data contained noise (e.g. the differential privacy example, or the citibike examples with many bins and/or few samples). The first example, using age data from a census area, demonstrated most clearly why this method may perform more accurately than the ‘centroid’ alternative; when the dataset has a peak or trough, the centroid method will fail to fully explain the bin integrals, and will have shallower responses to these changes than the data suggests is necessary. The reasons for its relative noise immunity are less clear, but maybe due to the noise-suppressing effect integration can have. Using the method to predict integrals (Section 4.4) was particularly effective, when compared to the centroid alternative. One immediate use case would be estimating the number of young adults from the age histogram, for example, for making local-shop stocking decisions, etc; the centroid method would massively underestimate the number of people in their mid-20s.

Briefly, we note that in some of the examples we model count data using a continuous output Gaussian Process. One could augment the model with a non-Gaussian likelihood function, but for pedagogical simplicity we used the standard Gaussian likelihood function.

Finally, in Section 3, we looked at approximation methods for non-cuboid, disjoint input regions. First we implemented the point-based approximation of Kyrriakidis (2004). Although it did not achieve a particularly practical RMSE on the census dataset, it beat the centroid alternative, and provides a principled method for handling such data. However it is likely to be restricted to lower-dimensional spaces due to the increasing number of approximation points required in higher dimensions. We then replaced the approximation built

of points with one built of rectangular patches, and used the covariance computed using the integral kernel. We found we needed considerably fewer rectangles than points to achieve similar accuracies. It is important to note though that the benefit from reduced numbers of training points is likely to be cancelled by the complexity of the integral kernel's covariance function, specifically the computation of four erfs in (2) and (3). However the relative advantages depend on the shape being approximated. Clearly an L shape will probably be more efficiently approximated by two rectangles than by many randomly placed points. Further improvements are possible for more complex shapes, as we haven't used the most efficient rectangle placement algorithm. Specifically, the rectangles could extend beyond the shape being approximated. One could introduce rectangles that contribute a negative weight, to delete those outlying regions, or cancel out patches where two rectangles have overlapped. We leave such enhancements for future researchers.

In this paper we have proposed and derived principled and effective methods for analytical and approximate inference over binned datasets. We have tested these methods on several datasets and found them to be effective and superior to alternatives. This provides an easy, useful and principled toolkit for researchers and developers handling histogrammed or binned datasets, who wish to improve their prediction accuracies.

References

- Alt H, Hsu D, Snoeyink J (1995) Computing the largest inscribed isothetic rectangle. In: Canadian Conference on Computational Geometry, pp 67–72
- Alvarez M, Luengo D, Lawrence N (2009) Latent force models. In: Artificial Intelligence and Statistics, pp 9–16
- Ažman K, Kocijan J (2005) Comprising prior knowledge in dynamic Gaussian process models. In: Proceedings of the International Conference on Computer Systems and Technologies, vol 16
- Cabello S, Cheong O, Knauer C, Schlipf L (2016) Finding largest rectangles in convex polygons. *Computational Geometry* 51:67–74
- Daniels KL, Milenkovic VJ, Roth D (1997) Finding the largest area axis-parallel rectangle in a polygon. *Computational Geometry* 7:125–148
- Dwork C, Roth A (2014) The algorithmic foundations of differential privacy. *Foundations and Trends in Theoretical Computer Science* 9(3-4):211–407
- Grimme C (2015) Picking a uniformly random point from an arbitrary simplex. https://www.researchgate.net/profile/Christian_Grimme/publication/275348534_Picking_a_Uniformly_Random_Point_from_an_Arbitrary_Simplex/links/553a08800cf247b858815a6b.pdf, University of Münster [Online; accessed 31-July-2018]
- Iacob P, Marinescu D, Luca C (2003) Covering with rectangular pieces. *Analele Stiintifice ale Universitatii Ovidius Constanta* 11(2):75–86
- Knauer C, Schlipf L, Schmidt JM, Tiwary HR (2012) Largest inscribed rectangles in convex polygons. *Journal of discrete algorithms* 13:78–85
- Kyriakidis PC (2004) A geostatistical framework for area-to-point spatial interpolation. *Geographical Analysis* 36(3):259–289
- O'Hagan A (1991) Bayes–Hermite quadrature. *Journal of statistical planning and inference* 29(3):245–260
- Ramsay JO (2006) Functional data analysis, Chapter 16. Wiley Online Library
- Riihimäki J, Vehtari A (2010) Gaussian processes with monotonicity information. In: Proceedings of the Thirteenth International Conference on Artificial Intelligence and Statistics, pp 645–652
- Stein P (1966) A note on the volume of a simplex. *The American Mathematical Monthly* 73(3):299–301
- Williams CK, Rasmussen CE (2006) Gaussian processes for machine learning. the MIT Press

Supplementary Material

Table 8 shows the RMSEs for the citibike results, while Figure 5 illustrates the error in the predictions for the census map dataset, comparing the results using either centroids or point-approximations.

Samples	Number of bins							
	1^4		3^4		7^4		15^4	
	centroid	integral	centroid	integral	centroid	integral	centroid	integral
160	636.0	636.4	619.7	640.5	663.1	624.1	1704.6	632.8
320	635.0	634.9	600.4	614.5	635.6	610.9	2416.1	629.0
640	635.8	635.3	590.0	581.4	627.7	591.8	1139.9	623.1
1280	636.0	635.5	589.8	571.4	610.6	602.8	793.9	606.5
2560	635.5	635.4	587.5	572.4	622.8	617.7	738.2	598.4

Table 8 Citibike: RMSE (in seconds) for the same experiment as reported in table 3.

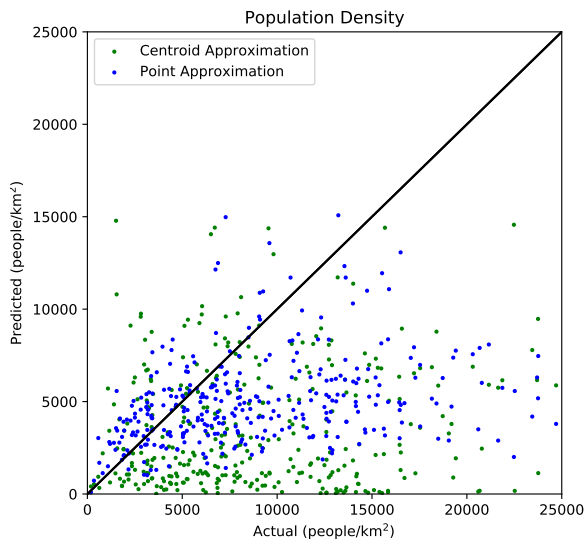


Fig. 5 Prediction accuracies on the 358 output areas tested for point-approximation vs using centroids. Both methods underestimate the densities, but the point approximation was somewhat more accurate.